Vol. 45, No. 2 (2023) 351-366, DOI: 10.24874/ti.1467.03.23.06

Tribology in Industry

www.tribology.rs

RESEARCH

Effect of Graphite Filling Pore Structure Size on the Tribology Behaviors of Tin Bronze/45 Steel Pairs With Grease Under Low-Speed and Heavy Load Conditions

Xiang Xu[a,b,c], Zekang Feng[a,b], Nengqi Xiao[a,b,c], Biao Liu[a,b], Xinze Zhao[a,b,c,*]

[a]*Hubei Key Laboratory of Hydroelectric Machinery Design & Maintenance, China Three Gorges University, Yichang, 443002, China,*
[b]*Hubei Engineering Research Center for Graphite Additive Manufacturing Technology and Equipment, China Three Gorges University, Yichang, 443002, China,*
[c]*National United Engineering Laboratory for Advanced Bearing Tribology, Henan University of Science and Technology, Luoyang, 471023, China.*

Keywords:

Tribological characteristics
Filled pore structure
Solid lubricant
Orthogonal test

* Corresponding author:

Xinze Zhao
E-mail: xzzhao@ctgu.edu.cn

Received: 27 March 2023
Revised: 24 April 2023
Accepted: 4 June 2023

A B S T R A C T

Copper-based solid lubrication inlay technology is widely used in industrial production, especially in low-speed and heavy load conditions, and the structure and distribution of the filling pore have a significant influence on the friction performance due to the distribution of contact stress. In this paper, based on the operating conditions of the bottom pivot of the Three Gorges gate, graphite is used as a solid filled lubricant. The effects of filling pore diameter, filling pore depth, and area distribution rate on the friction and wear properties were studied by orthogonal equivalent test on MMW-1A tester with grease. Combining the three-dimensional morphology test and ferrography analysis, the results show that: 1) the influence of three parameters on the test results are: filling pore diameter > area distribution rate > filling pore depth; 2) when the filling pore diameter is 3 mm, the area distribution rate is 12%, and the filling pore depth is 0.5 mm, which is the equivalent the optimal structure of the filling pore size under working conditions. According to this conclusion, the actual filling structure can be obtained based on the similarity theory. As Coulomb friction is material and contact stress related, the calculation of the stress distribution during dynamic operation is difficult and therefore the analysis is carried out experimentally.

1. INTRODUCTION

The use of solid lubricating powder or lubricating film to minimize friction and wear between two bearing surfaces with relative motion is referred to as solid lubrication. Solid lubricants have low shear strength and are easy to adhere to the friction surface, allowing them to form a continuous and stable lubricating film on the surface of the friction pairs. This reduces the friction and wear of the friction pairs. Common solid lubricants include MoS_2, graphite, nylon, etc. [1-3]. It is used in the bottom pivot of the Three Gorges gate because it has the advantages of poor pollution and is not easy to cause leakage. Currently, a large number of miter gates suffer from structural damages due to excessive bottom pivot wear [4]. So this paper investigates a specific operating condition (the gate bottom pivot problem) for which there is currently either no research or the current research is insufficient to solve the existing engineering problem.

Excessive specific pressure and inadequate lubrication of the friction pairs are essential causes of wear in bottom pivot operation [5]. Many scholars have started studies for this reason. Hamilton [6] first suggested in the 1960s that improved friction properties between friction subsurface could be achieved through surface-filled pores. Yu [7] implemented the Successive Over-Relaxation method to determine the average hydrodynamic pressure created by various texture patterns with dimples in the shapes of circle, ellipse, and triangle at different orientations to the direction of sliding. The results showed that the geometric shape and orientation of the textures had a significant impact on the load-carrying capacity of the contacting surfaces. Considering the effect of contact surface geometry on wear, Hua [8] investigated the frictional behaviour and lubrication mechanism of self-lubricating Gr-MoS_2-PI-CNT composite, the results indicate that the dimples filled with composite solid lubricant (sample TPL) exhibited the best lubrication mechanism with the lowest friction as compared to the smooth surface without lubrication (sample S), textured surface without lubrication (sample T), textured surface burnished with solid lubricant (sample TSL) and textured surface coated with solid lubricant block (sample TBL). Yang [9] studied the effects of microtexture preparation parameters by detecting elements in the area around the microtexture. Through friction experiments, the relationship between different microtexture preparation parameters and the surface wear rate of cemented carbide was studied. C.E.Morstein [10] investigated the primary wear mechanism of graphite under high mechanical loads by sliding friction. Chen [11] measured the coefficients of friction and wear volume of the laser dimple textured surfaces and the hardness of the dimple edge. The worn surfaces of the specimens were examined, and the elemental contents of the wear debris were analyzed. Joko [12] designed the structure of a round disk wear tester and prepared a series of specimens to find out the effect of graphite lubrication on the degree of wheel and railroad wear and to minimize the wear effect of friction. It was shown that the more the volume of graphite polished to the surface of the wheel specimens, the less the material loss due to surface contact in different books of graphite filled in the filling pores on the surface of the wheel specimens. Ryk [13] in order to investigate the effect of the filled pore structure on the frictional properties of the piston/cylinder liner, the piston was machined with a filled pore structure at local locations and subjected to frictional wear tests. Shi [14] prepared graphite-like carbon (GLC) films of different thicknesses on the surface of 316L stainless steel, using closed field unbalanced magnetron sputtering system to investigate the influence of film thickness on the micro-structure, mechanical and tribological properties. A.Codrignani [15] studied numerically and experimentally the effect of operating conditions on surface texture shape parameters in determining the optimal texture shape in terms of friction reduction and load-carrying capacity. Guo [16] numerically analyzed the effect of the axial location of the contact zone on the sealing performance of lip seals with different filler pore texture shapes. They showed that the triangular filler pore texture shape produces a positive pumping rate regardless of the location of the contact zone on the shaft surface.

In order to investigate the influence of graphite's granulometry on the dry sliding behavior of a copper-free friction material against pearlitic

cast iron, Mara [17] obtained comparing specific characteristics (i.e., morphology and chemical composition) of the friction layers formed on each friction material under the different testing conditions. Zhao et al. [18,19] used the UMT-2 multifunctional friction and wear tester to conduct a pin-disk friction sub-test to simulate the low-speed heavy load working conditions of the gate bottom pivot. They investigated the effect of graphite particle size on the friction and wear performance of the gate bottom pivot friction sub-test. And through theoretical calculations, the relationship between the measurement error and the number of grooves and the distribution of grooves for different diameter friction subsets is derived.

In addition, the incorporation of solid lubricants and appropriate reinforcing phase particles into the copper matrix can be employed to create self-lubricating copper-based composite coatings, which can substantially enhance the frictional and wear-resistant efficiency of copper-based coatings [20]. The bottom pivot shaft of the Three Gorges gate is made of copper-based inlay material. Zhao et al. [21] were carried out the friction and wear tests: 45# steel (carbon steel) was rubbed with aluminum bronze, aluminum bronze-based inlaid solid self-lubricating bearing (ISSLB) material, tin bronze, and tin bronze-based ISSLB material under different loads. The friction and wear performance of the composites were analyzed using a pin-on-disc tribometer. Sarmadi [22] indicated that the friction coefficients of the composites were lower than those of pure annealed copper, and decreased with an increase in graphite content. Zhang [23] analyzed the effects of ball milling time on the material's microstructure and properties. The dry friction properties of the material were tested using a pin-on-disc contact reciprocating test machine under a load of 200N. The test results showed that the copper-based material containing FeS exhibited better anti-friction and anti-wear properties, and that the friction coefficient of the friction pair was lower and more stable. The aim of this study was to investigate the effects of a graphite-MoS_2 composite solid lubricant on the tribological properties of copper-based bearing materials under dry conditions. To achieve this, a mixture of graphite-MoS_2 was inlaid into ZQSn6-6–3 tin bronze and ZQAl9-4 aluminum bronze matrices. These copper-embedded self-lubricating bearing materials were used in friction pairs with 2Cr13 stainless steel, and their tribological properties were studied using an MM200 wear test machine [24]. In order to fabricate a FeS/Cu-Bi copper-based lead-free bearing material to maintain good friction-reducing and anti-adhesive properties under boundary lubrication conditions, Yin [25] utilized mechanical alloying and powder metallurgy techniques to fabricate the material, which was then subjected to dry friction tests using an HDM-20 wear tester. The results showed that mechanical alloying can improve the antifriction and wear resistance of the materials. Sarath [26] conduced that the tribological performance of silicone rubber/graphite(QMG) composites were found to be in agreement with its morphological, mechanical and dielectric properties.

In order to improve the optimized performance of the filling pore and extend the maintenance cycle of the gate bottom pivot. In this paper, we take the bottom pivot of the Three Gorges gate as the research object and carry out the research on the effect of graphite-filled pore structure size on the tribological performance under low speed and heavy load conditions. Using tin bronze and 45 steel as paired sub-materials [27], frictional wear orthogonal tests were carried out by studying three parameters, different pore diameters, area distribution rates, and pore depths, combined with three-dimensional morphological techniques and ferrography analysis.

2. EXPERIMENTAL MATERIALS AND METHODS

2.1 Test device

Adopt MMW-1A vertical universal friction and wear tester for friction and wear test. The testing machine has a loading force range of 10 N~1000 N, the spindle speed range of $5r/\text{min}\sim2000r/\text{min}$, and a variety of friction pairs installation methods such as pin discs, ball discs, and thrust rings. The pin-disc wear test is used in this experiment. The upper sample is the sample pin of $\phi5\times13mm$, and the material is 45# steel; the lower model is the sample disc of $\phi54mm-\phi16\times9mm$, and the material is tin bronze. The distance between the center of the disc sample and the center of the pin sample is 14 mm, as shown in Figure 1.

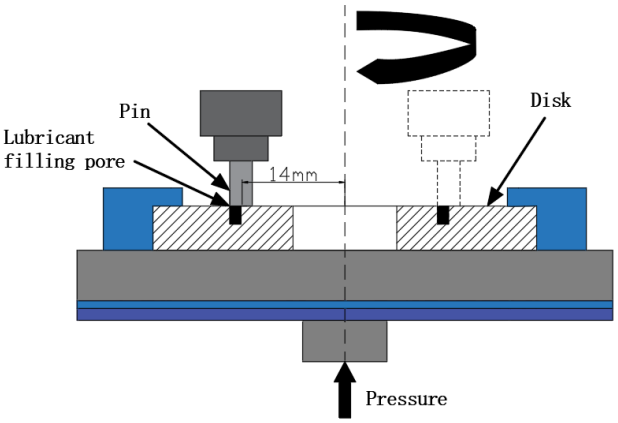

Fig. 1. Filling pore distribution and test loading scheme.

2.2 Test condition

The average mass of the Three Gorges miter gate is 850 tons, and the height *H(m)* and the width *L(m)* of a single-door leaf are nearly 38.5 m and 20.2 m, respectively. So according to Fig. 2, the force on the bottom pivot could be calculated as follows:

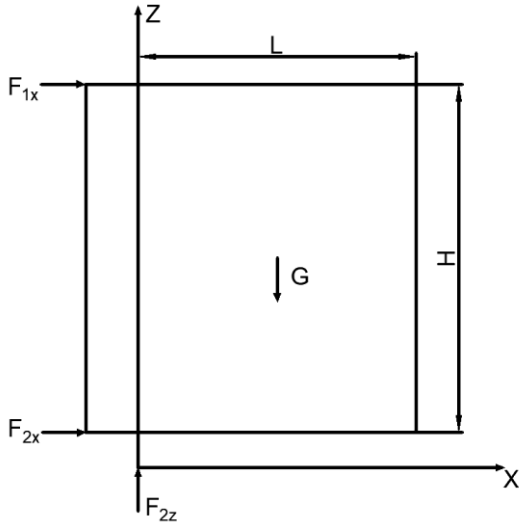

Fig. 2. Schematic diagram of the miter gate structure.

$$F_{1x} = -F_{2x} = G \cdot \frac{L}{2} / H \tag{1}$$

$$F_{2z} = G \tag{2}$$

$$F_2 = \sqrt{F_{2x}^2 + F_{2z}^2} \tag{3}$$

$$\theta = \arctan(F_{2x} / F_{2z}) \tag{4}$$

Where *G(mg)* is the gravity of the miter gate, $\theta(°)$ is the angle between the resultant force and the *Z -axis*. And the radius *R(mg)* of the bottom pivot is 0.5 m, so the maximum contact stress could be calculated as follows:

$$\sigma(\theta,\varphi) = \frac{3F}{2\pi \times r^2 (1-\sin^3 \varphi)} \cos\theta \tag{5}$$

Where $\varphi(°)$ is the angle between the projection of the resultant force on the horizontal plane and the *X-axis* in the spherical coordinate system, when $\varphi = 0$, the maximum contact stress $\sigma_{\max} = 16.3MPa$.

The operating angle and time are about 70° and 40s, so the maximum linear velocity $v_{\max} = 0.0152m/s$ are obtained by calculation. According to the sample structure of the testing machine, assuming that the area of the pin is the proper contact area, the test load $F \approx 320N$ and the test speed $n \approx 10r/\min$ could be obtained.

2.3 Filled pore structure

There are a large number of solid lubricant filling pores with a diameter of 40 mm and a depth of 10 ~ 15 mm settings on the bottom pivot bearing bush of the Three Gorges miter gate. The surface area of the whole filling pore accounts for about 14% of the hemispherical surface area of the bearing bush. According to the similarity theory, the corresponding test structure parameters are designed, as shown in Table 1.

Table 1. Orthogonal test level factor table.

Level	Factor		
	A diameter/ (mm)	B area distribution/ (%)	C depth/ (mm)
1	3	12	0.5
2	2.5	14	1
3	2	16	1.5

Taking a sample with a pore diameter of 3 mm, pore depth of 0.5 mm, and a distribution ratio of 12% as an example, the pores are designed to be evenly distributed in two circles (one inside and one outside) to ensure full contact between the solid lubricant and the pin sample, while avoiding interference between adjacent filled pores. The two closest filled pores are set at a 10° angle relative to the rotation center, where the thickness of the disc specimen is 9mm. The 3D diagram is shown in Figure 3(a), and the 2D diagram is shown in Figure 3(b).

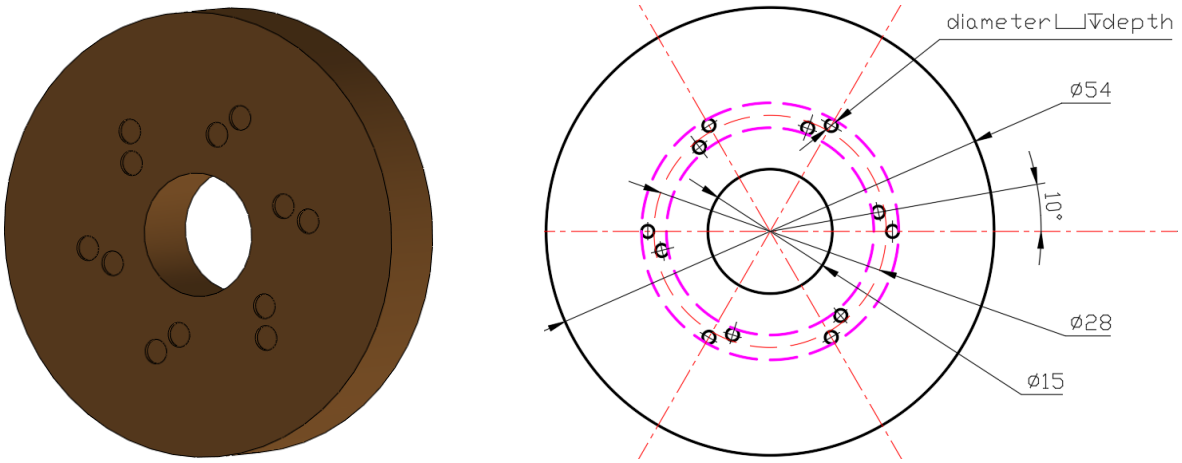

(a) (b)

Fig. 3. Structure of the filling pore a-the 3D diagram, b-the 2D diagram.

In order to reduce the test times and ensure the reliability of the test data, the orthogonal test is used to determine the optimum filling pore structure parameters. The factor level table of the orthogonal test is shown in Table 2.

Table 2. Three-factor orthogonal test table.

Order	Test Arrangement		
	A diameter / (mm)	B area distribution / (%)	C depth / (mm)
1	1 (3)	1 (12)	1 (0.5)
2	1	2 (14)	2 (1)
3	1	3 (16)	3 (1.5)
4	2 (2.5)	1	2
5	2	2	3
6	2	3	1
7	3 (2)	1	3
8	3	2	2
9	3	3	1
K_1	28.7	4.34	5.34
K_2	7	25.7	25.37
K_3	9.34	15	14.33
$\overline{K_1}$	9.56	1.45	1.78
$\overline{K_2}$	2.33	8.57	8.46
$\overline{K_3}$	3.11	5	4.78
R	7.23	7.12	6.68

When the level number is the same as i in the same column, the K_i in the table reflects the sum of the test results. While $\overline{K_i} = K_i / n$ represents the number of levels in the table, n shows the number of groups. The stark contrast R is the difference between the highest and minimum value of $\overline{K_i}$ of the relevant factor and shows the magnitude of the change in the factor's level value during the test. The value of R reflects the magnitude of the factor's effect on the test outcomes. R may be used to identify the amount of the effect of the three parameters on the test results in the test process since the larger the value indicates, the greater the influence of the factor on the test results. As a result of the table, it is possible to deduce that: filling pore diameter > area distribution rate > filling pore depth.

2.4 Sample preparation and test process

After mixing graphite with a binder in a certain proportion (16%), mixed solid lubricant is formed, and then the solid lubricants are filled into the filling pore of the sample disc. Then placed the sample disc (which can be multiple pieces together) on the mounting splint. The lower clamping plate contacts the bottom of the sample disc, pasted heat insulation paper between the upper clamping plate and the sample disc, and the upper and lower clamping plates are fixed with bolts. After constant temperature curing at 80°Cfor 12 h, removed the clamping plate. Then, the sample disc shall be polished with 400# sandpaper to remove the excess mixed solid lubricant coating on the surface of the sample, and then cleaned the sample disc with an ultrasonic cleaner using absolute ethanol as the cleaning agent. Grind and polish the surface of the sample again, make the roughness of the sample disk surface (Ra) less than 1.6μm, clean again to obtain the sample required for the equivalent test, as shown in Fig. 2. Install the pretreated sample pin and sample disc at the corresponding position of the friction and wear tester, and applied the 1# lithium grease on the upper surface of the sample disc and the lower surface of the sample pin. After installation and application, the loading test was carried out according to the calculated working conditions, and each test time was 1 h.

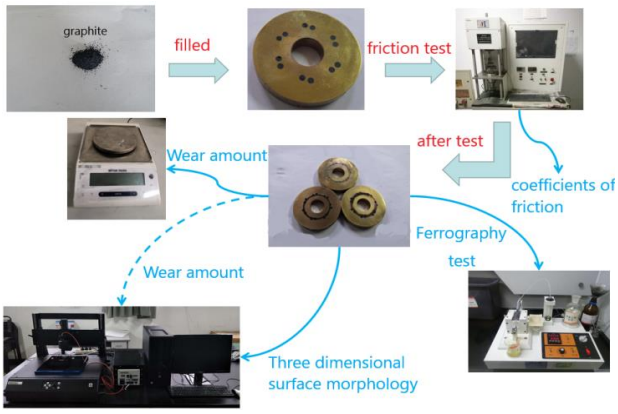

Fig. 4. Friction and wear test scheme.

For wear specimens, firstly, the mass of the sample disk is weighed with an electronic balance and recorded before the test. Secondly, the weighed sample is placed on the friction and wear tester for the friction and wear test. After the test, the grease on the specimen is collected and used for ferrography analysis. Following an ultrasonic cleaning, anhydrous ethanol is used to remove any remaining pollutants from the specimen, which is then dried in the drying oven. Reweighing and recording the dried specimens are done once more. The difference in mass before and after the test is the amount of wear $\Delta m(mg)$.

3. ORTHOGONAL TEST RESULTS AND ANALYSIS

For comparative testing and data analysis, the previously mentioned test conditions are used: a pore diameter of 3 mm, a pore depth of 0.5 mm, and an area distribution rate of 12%. The specimens were analyzed for friction coefficient, three-dimensional surface morphology, wear quantity, wear depth, and ferrography analysis before and after the wear comparison.

3.1 Friction coefficient

The friction coefficient is automatically recorded by the friction and wear tester. Figures 5 to 7 show the variation curves of friction coefficient with time for different pore diameters, area distribution rates, and pore depths within 1 h. Based on the magnitude of the effects of the three parameters derived from the test, the effect of pore diameter on friction performance is first analyzed. All other conditions were kept constant (12% area distribution rate and 0.5 mm pore depth), and the pore diameter was varied to investigate the effect on friction performance. The friction coefficients for different pore diameters were showed in Figure 5.

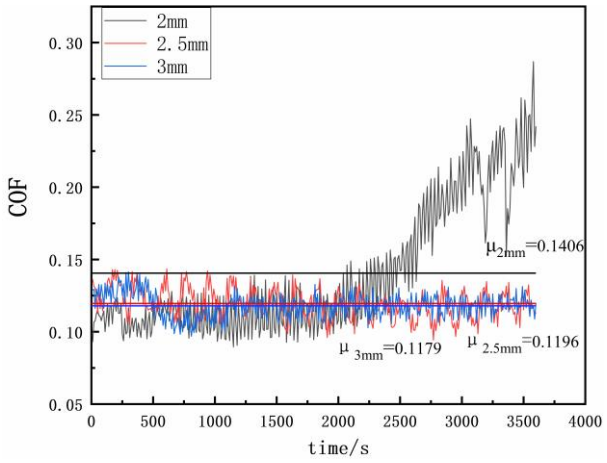

Fig. 5. Friction coefficient at different pore diameters.

As shown in Figure 5, when the pore diameter is used as the variable, the friction coefficients of specimens with pore diameters of 2.5 mm and 3 mm do not change significantly over time, and do not exhibit large fluctuations. In contrast, the friction coefficient of the specimen with a pore diameter of 2 mm does not exhibit large fluctuations before 2500 s, but suddenly rises sharply after 2500 s, accompanied by a wide range of changes. The average friction coefficients of the three specimens over a span of an hour were 0.1196, 0.1179, and 0.1406, respectively.

Next, the effect of area distribution rate on friction performance was analyzed. The effect of varying the area distribution rate on the friction performance was analyzed with the remaining conditions (pore diameter 3 mm, pore depth 0.5 mm) remaining unchanged. The friction coefficients for different area distribution rates were showed in Figure 6.

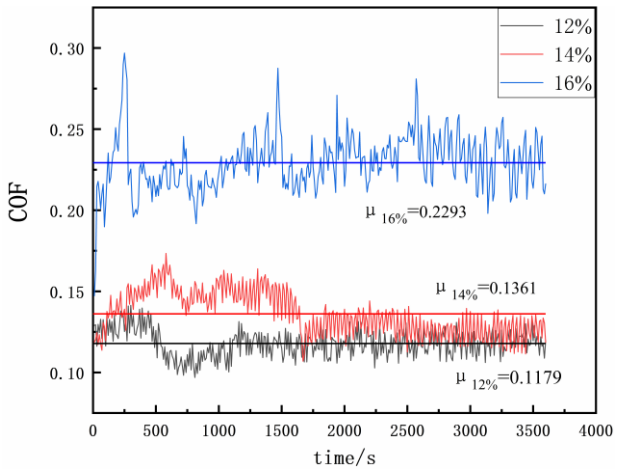

Fig. 6. Friction coefficient at different area distribution rates.

As can be seen from Figure 6, when the area distribution rate is used as the variable, with the passage of time, the overall vibration frequency of the specimen with an area distribution rate of 16% is more intense, and its friction coefficient is significantly larger than that of the specimen with an area distribution rate of 12% and 14%; the specimen with an area distribution rate of 12% has a decreasing trend at 500 s and returns to stability at the 1200 s, and it is overall the average coefficient of friction of the specimen with 12% area distribution tended to stabilize after 1200 s. The overall coefficient of friction fluctuated more slowly. While the specimen with 14% area distribution showed a slight increase in the early stage and gradually recovering to a steady state after 1700 s. The average coefficients of friction of the three specimens within 1 h were 0.2293, 0.1179, and 0.1361, respectively.

Finally, the effect of pore depth on friction performance was analyzed. The effect of the pore depth on the friction performance is investigated by varying the pore depth while keeping the rest of the conditions constant (pore diameter of 3 mm and area distribution rate of 12%). The friction coefficients for different filling pore depths were showed in Figure 7 .

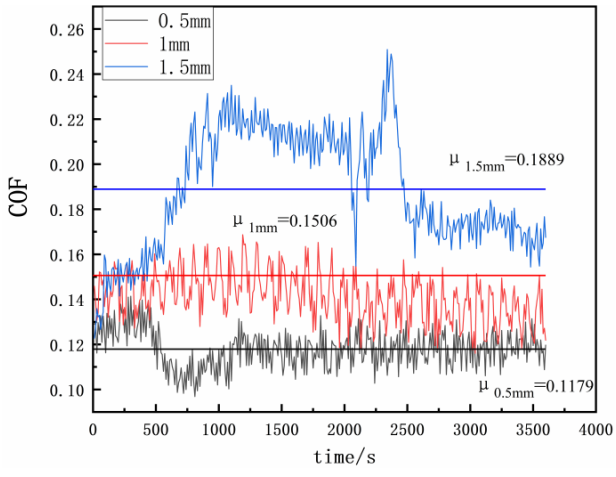

Fig. 7. Friction coefficient at different filling pore depths.

As shown in Figure 7, when the pore depth is used as the variable, the average friction coefficient of the specimen with a pore depth of 1.5 mm increases significantly more than that of the specimens with a pore depth of 0.5 mm and a pore depth of 1 mm over time. It exhibits a sharp upward trend before 1200 s, stabilizes between 1200 s and 2000 s, then sharply declines before rising again, and the overall vibration frequency is very violent. In the early stages of operation, in the wear and tear phase, the coefficient of friction changes considerably; later on it shows a certain regularity and is considered to reach stability; the overall fluctuation of the specimen with 0.5 mm pore depth is not significant, with a slow decline in the 500 s followed by a slow rise in the 750 s before stabilizing after 1200 s; the overall fluctuation of the specimen with 1 mm pore diameter is insignificant, and its overall friction coefficient is also between the two. The average friction coefficients of the three specimens in 1 h were 0.1889, 0.1179, and 0.1506, respectively.

3.2 3D morphology and Wear quantity

The ST400 3D surface morphology was used to analyze the abrasion marks. The effects of different pore diameters, pore depths, and area distribution rates on the structure of filled pores were analyzed by scanning the abrasion marks. The scanning area is 4mm×4mm, the step length is 20μm, and the sampling frequency is 200Hz.

Figure 8 presents the three-dimensional morphology by scanning the area of the abrasion marks under different parameters. For comparison, the bottom of their specimens is made uniformly as a reference. In Fig. 8(a), (b) and (c) correspond to the three-dimensional morphology for different pore diameters, different area distribution rates, and different pore depths. In Fig. 8(a) A, B, and C correspond to the specimens with 2 mm, 2.5 mm, and 3 mm pore diameters. In Fig. 8(b) A, B, and C correspond to the specimens with 12% area distribution, 14% area distribution, and 16% area distribution. In Fig. 8(c) A, B, and C correspond to the specimens with pore depth of 0.5 mm, pore depth of 1 mm, and pore depth of 1.5 mm. The final results are averaged by measuring the values over several trials. By comparing the 3D morphology map of the unworn parts of the scanned related parameters, the final surface morphology characteristics parameters before and after the wear for various pore diameters, area distribution rates, and pore depths are shown in Tables 3 to 5.

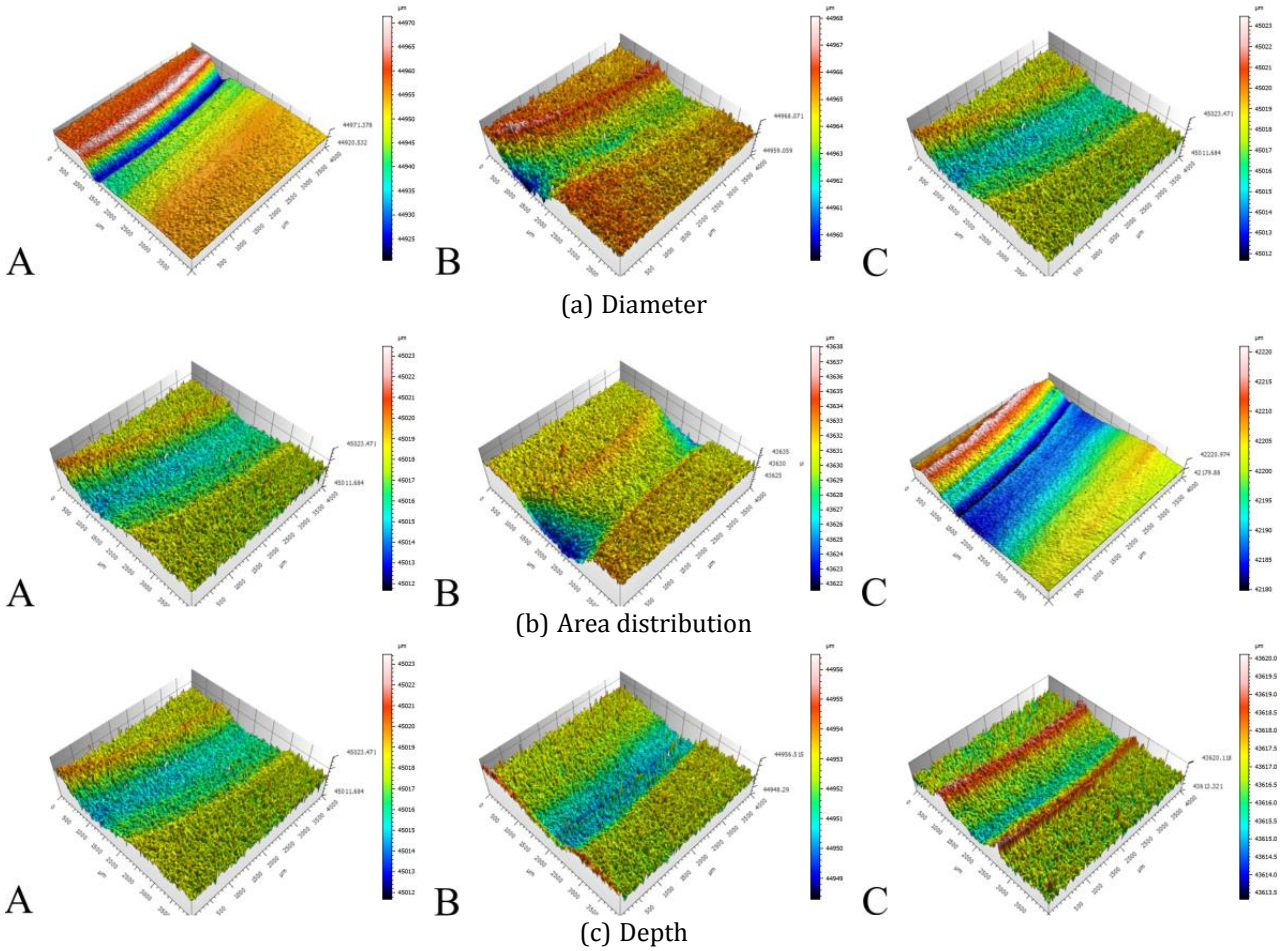

Fig. 8. Three-dimensional morphology.

Table 3. Values of surface morphology parameters with different pore diameters.

Pore diameters	*Sa* (*μm*)		*Sq* (*μm*)		*Sz* (*μm*)	
	Unworn	Worn	Unworn	Worn	Unworn	Worn
2 mm	0.701	7.156	0.891	9.485	7.563	44.469
2.5mm	0.316	0.797	0.414	1.049	4.604	5.441
3 mm	0.425	0.984	0.539	1.181	4.501	7.461

The surface root means *sq*uare value Sq, surface arithmetic means *Sa*, and maximum height *Sz* of the three specimens following wear demonstrated an increasing tendency compared to the unworn specimens, as shown in Table 3. The largest difference in figures before and after wear was observed for the specimen with a 2mm pore diameter, where the *Sa* value increased by 6.46μm, the *Sq* increased by 8.59μm and the *Sz* increased by 36.91μm. This condition could be caused by the fact that less mixed solid lubricant is kept in the specimen with a smaller aperture diameter. The mixed solid lubricant between the friction subsets is not supplied in time as the mixed solid lubricant consumption in the filled pore grows with time. As a consequence, the coefficient of friction of the specimens with apertures of 2 mm increases rapidly.

Table 4. Values of surface morphology parameters with different area distribution.

Area distribution	*Sa* (*μm*)		*Sq* (*μm*)		*Sz* (*μm*)	
	Unworn	Worn	Unworn	Worn	Unworn	Worn
12%	0.425	0.984	0.539	1.181	4.501	7.461
14%	0.38	1.1	0.482	1.627	4.374	7.589
16%	0.35	7.51	0.457	8.796	4.167	29.324

As can be seen in Table 4, all three specimens show a rising trend, The specimens with an area distribution of 16% had a large difference in values before and after wear, with *Sa* value increased by 7.16μm, *Sq* by 8.34μm and *Sz* by 25.16μm. The situation is when the area distribution rate is significant, resulting in a large area of mixed solid lubricant, on the one hand, will reduce the overall hardness of the entire disk specimen friction surface, on the other hand, will also lead to an increase in the disk test friction surface roughness, and both of these aspects will lead to poorer friction performance.

Table 5. Values of surface morphology parameters with different pore depths.

Pore depths	*Sa* (*μm*)		*Sq* (*μm*)		*Sz* (*μm*)	
	Unworn	Worn	Unworn	Worn	Unworn	Worn
0.5mm	0.425	0.984	0.539	1.181	4.501	7.461
1 mm	0.326	0.75	0.415	0.947	3.485	5.893
1.5mm	0.943	0.658	1.198	0.861	10.943	6.186

Table 5 shows that all parameters of the specimen with a pore depth of 1.5 mm show a decreasing trend compared to the specimens with a pore depth of 0.5 mm and 1 mm. Its *Sa* value decreased by 0.28*μm*, *Sq* by 0.34*μm* and *Sz* by 4.76*μm*. The possible reason for that it is not the case that a specimen with a large area distribution is good, but on the contrary the larger the area distribution the more likely it is that secondary wear of the specimen by abrasive particles between the friction pairs will occur.

For wear specimens, only the wear amount of the disk specimen is tested because the pin and disk test is a soft and hard contact, and there is almost no wear for hard pins. The wear quantity of the three parameters in 1 h is shown in Figure 9.

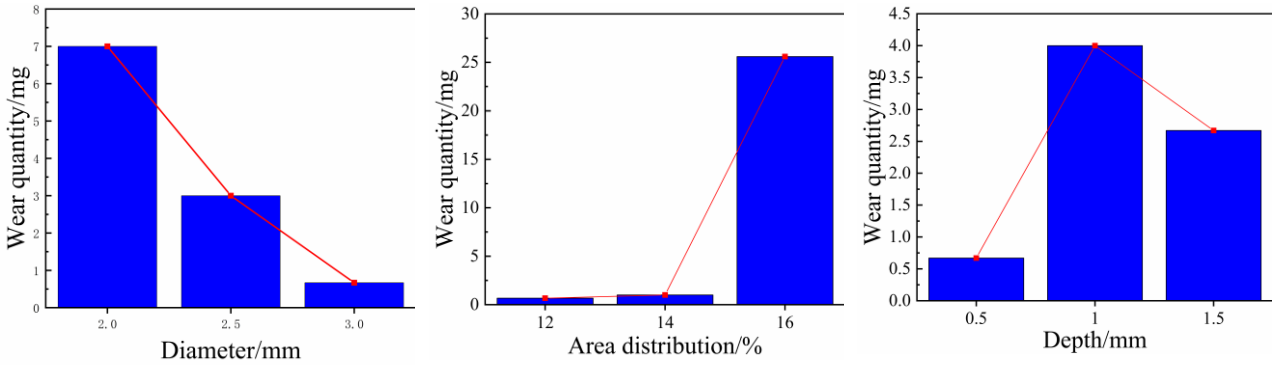

Fig. 9 Wear of the three parameters in 1h.

As can be seen in Fig. 9(a), the wear of the disk specimen exhibits a decreasing trend with an increase in pore diameter. With the continuous progress of the test, a small fraction of the stored specimens become incapable of delivering a blended solid lubricant to the surface of the friction pairs, thereby resulting in an escalation of wear and tear. In contrast, many storage specimens can continue to provide mixed solid lubricant to the surface of the friction pairs, resulting in correspondingly smaller wear. The amount of mixed solid lubricant that can be stored depends on the filling pore's diameter. From Fig. 9(b), the wear of the disk specimen shows an increasing trend with the increase of the area distribution rate. When the area distribution rate is 16%, the wear of the disk specimen is much larger than the wear of the remaining two specimens. The possible reason is that although the mixed solid lubricant is stored in the filled pores with an area distribution rate of 16% more, it will decrease the hardness of the contact surface of the disk specimen and increase of the surface roughness. This results in lower friction performance for the disk specimen and is more likely to be brought on by secondary wear brought on by abrasive particles between the friction pairs. The wear amount is the smallest among the three at a pore depth of 0.5 mm, as

shown in Fig. 9(c), and this is also the trend for the friction coefficient. Discussed in terms of both stress deformation and lubrication coefficient: less vertical stress deformation with less depth; more lubricant extrusion with more depth for lubrication. The wear amount might be because the disk specimen exhibits more extraordinary friction performance when the pore depth is shallow. When put through a frictional wear test, it performs well in terms of wear resistance and reduction.

3.3 Wear depth

Since the wear quality is related to the density of the filling material, we are more concerned with the wear depth from the point of view of wear loss efficiency. Therefore, the wear depth analyzed by combining the data of 3D morphology. These three cross-sections were taken in the radius direction of the worn pin disc specimen, and the adjusted relative surface heights were plotted as shown in Figure 10.

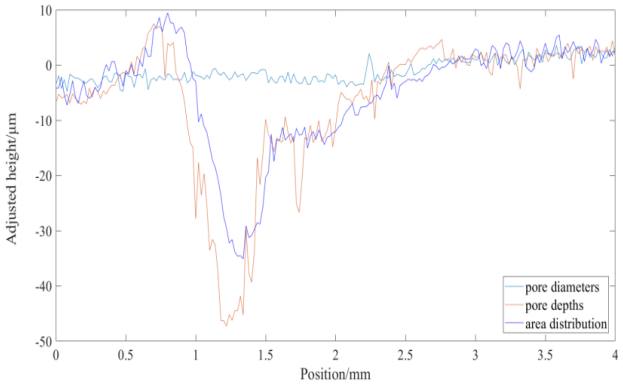

Fig. 10. Wear depth of lower disc specimens influenced by different parameters.

Since the scanned cross-sectional locations have differences, but the height of their unworn areas is approximately the same, the wear depth is defined as:

$$\Delta H = \sum \frac{H_h}{N_h} - \sum \frac{H_l}{N_l} \tag{4}$$

Where H_h and H_l denote the relative heights of the unworn and worn parts, respectively. Where H_h indicates the data of the highest point of the radial position of the highest two points of any curve in the graph, N_h and N_l indicate the number of points measured on the surface of the unworn and worn parts, respectively. From this, it can be calculated that:

$$\Delta H_1 = 1.0226 \mu m; \Delta H_2 = 6.5353 \mu m; \Delta H_3 = 5.0659 \mu m.$$

As can be seen from the figure, the front and rear heights of the unworn parts before and after wear are approximately the same, where the mutual extrusion between the pins and discs in the test caused a bulge in the disc specimen near wear. Where the bulge in the specimen affected by the pore depth is more significant compared to the factor of area distribution rate. In the specimen affected by the pore diameter, the surface height did not show a wide range of fluctuations. It is presumed that the possible reason is that during the wear process, the graphite grain size ruptured and formed a lubricating film, so its lubrication effect is better. The specimens affected by the other two parameters are presumed to have plastic deformation during the wear process, so their relative surface height is larger. The wear depths of the specimens affected by the three parameters are shown in Table 6. As can be seen from Table 6, both in terms of wear quality as well as wear depth, the specimens affected by the pore diameter have the least amount of wear, and the specimens affected by the pore depth have the most amount of wear.

Table 6. Wear of lower disc specimens affected by different parameters.

	Wear depth $\Delta H / \mu m$	Wear quality $\Delta m / mg$
Pore diameter	1.0226	0.67
Pore depth	6.5353	3
Area distribution rate	5.0659	1

3.4 Ferrography analysis

The wear products were examined and analyzed using an FFM3 ferrography analysis spectrometer and a BX51 microscope. Figures 11 to 13 show the ferrography analysis for different pore diameters, different area distribution rates, and different pore depths. Among them, the ferrography analysis at different pore diameters is shown in Figure 11.

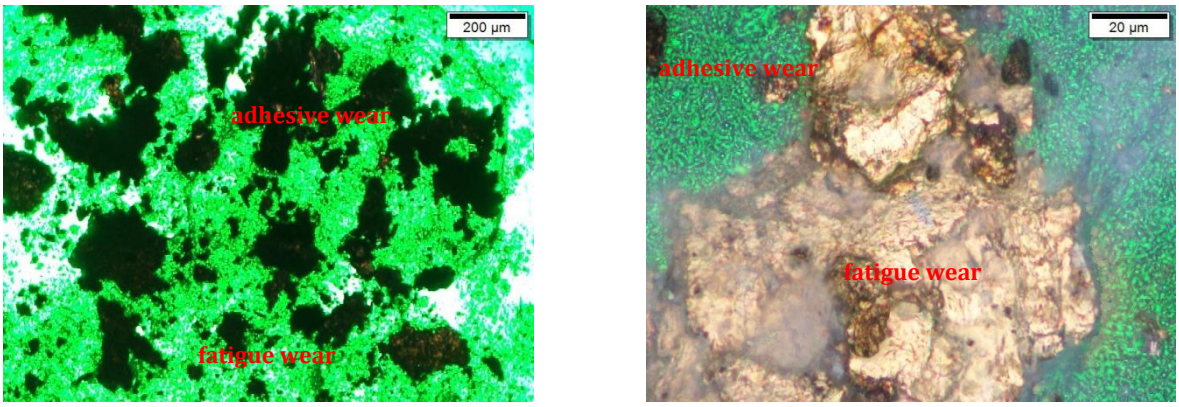

(a) Ferrography analysis with 2 mm pore diameter

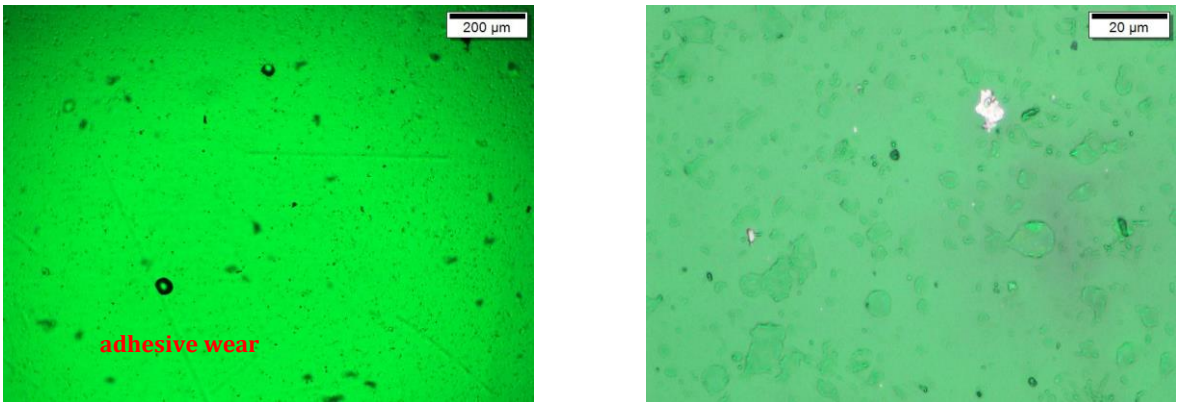

(b) Ferrography analysis with 2.5 mm pore diameter

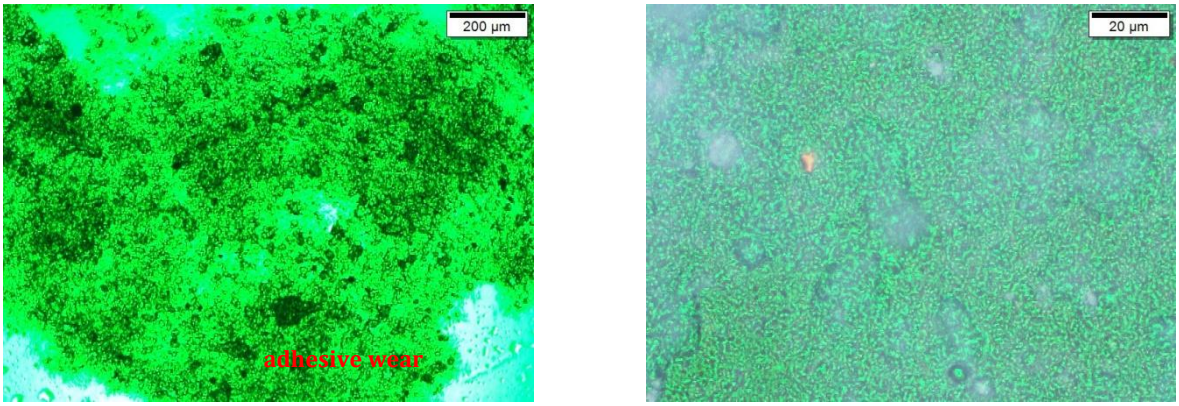

(c) Ferrography analysis with 3 mm pore diameter

Fig. 11. Ferrography analysis at different pore diameters.

The ferrography analysis of the corresponding pore diameters is shown in Fig. 11(a), (b), and (c), and it is discovered that the particle size of the abrasive grains decreases as the pore diameter of the filled pore grows, following the same rule as that of wear amount. When the filling pore aperture is 2 mm, the larger abrasive particle size is shown in conjunction with the ferrography analysis. The particle size of a few abrasive particles is even more significant than 50μm, and adhesive wear is the primary type of wear among two others, including fatigue wear. When the aperture diameter is 2.5mm, the abrasive particle size is smaller than when the aperture diameter is 2mm; there are only individual abrasive particles larger than 10μm and none more significant than 50μm, and the kind of wear is light adhesive wear. When the aperture is 3 mm, the size of the abrasive particles is slightly smaller than the size of the abrasive particles when the aperture is 2.5 mm, and there are only individual abrasive particles with a size greater than 10μm, and no abrasive particles with a size greater than 50μm exist, and the form of wear is individual adhesive wear. Figure 12 shows the ferrography analysis at different area distribution rates.

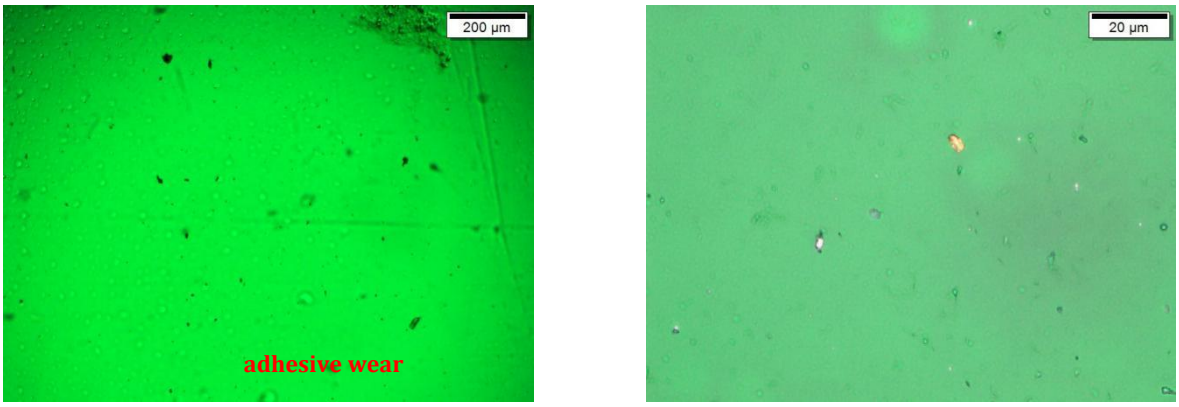

(a) Ferrography analysis at 12% area distribution

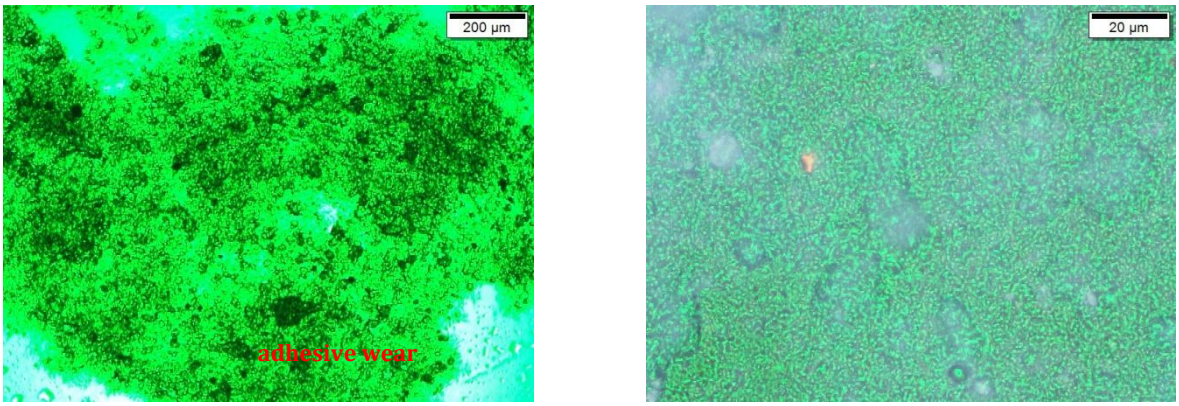

(b) Ferrography analysis at 14% area distribution

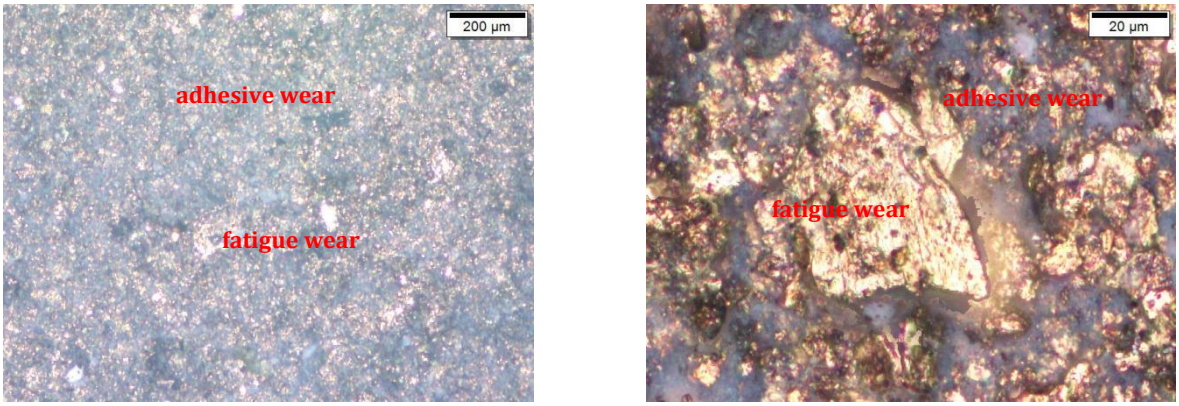

(c) Ferrography analysis at 16% area distribution

Fig. 12. Ferrography analysis at different area distribution rates.

As the area distribution rate increases, the particle diameter of the abrasive grains formed during the test also increases, according to the ferrography analysis of the corresponding area distribution rate shown in Fig. 12(a), (b), and (c). Combined with the ferrography analysis, it is determined that the abrasive grains have a tiny particle diameter when the area distribution rate is 12%. Only a small number of abrasive grains have a particle diameter larger than 10μm, and they only wear a little adhesive wear. The abrasive particle diameter is slightly greater than 12% when the area distribution rate is 14%. The wear occurs in slight adhesive wear, and there are few abrasive particles with a particle diameter bigger than 10μm and none with a particle diameter more significant than 50μm. The particle diameter of its abrasive grains when the area distribution rate is 16% is obviously larger than the size of the first two abrasive grains. In addition to changing from the adhesive wear of the first two to more complicated composite wear that includes adhesive wear and fatigue wear, there are individual abrasive grains with a particle diameter larger than 50μm. Figure 13 shows the ferrography analysis at different filling pore depths.

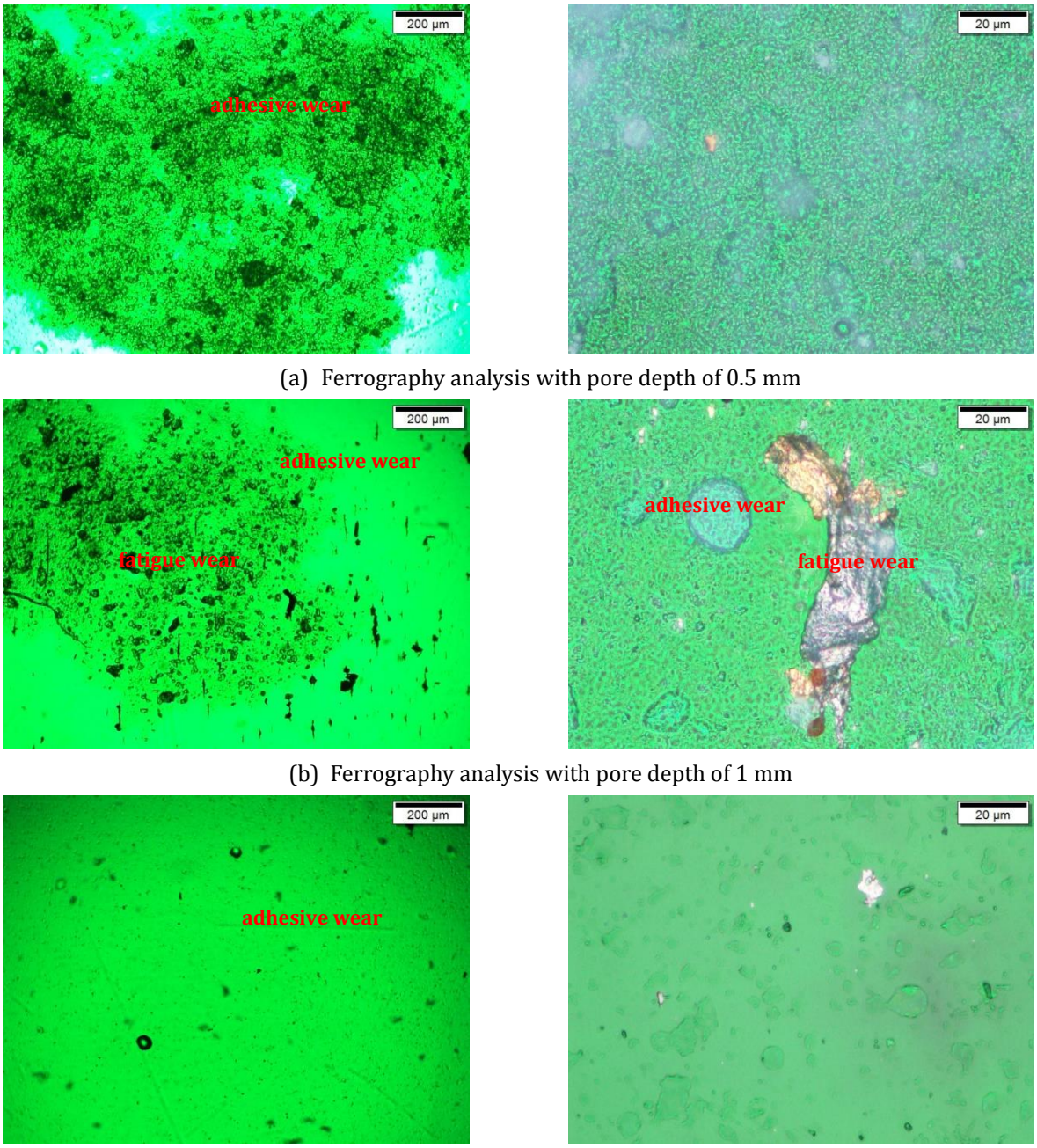

Fig. 13 Ferrography analysis at different filling pore depths.

The ferrography analysis of the corresponding depths is shown in Figures 13(a), (b), and (c), and it is discovered that as the filling pore depth changes, so does the particle diameter of the abrasive grains produced during the test. When the depth of the filling pore is 0.5 mm, the particle diameter is the smallest, and there are only a few particles with a particle diameter larger than 10μm. The wear is only in the form of slight adhesive wear, it is discovered using the ferrography analysis. At a depth of 1 mm, the grain size is slightly larger than that of a 12% area distribution, and there are only a few grains with a grain size greater than 10μm. The pictures show that there are grains with a grain size greater than 50μm, and there is high temperature oxidation, and the form of wear is a combination of adhesive wear and fatigue wear. There is no grain size of more than 10μm in the grain, and only one adhesive wear occurs when the pore depth is 1.5 mm. The grain size is larger than the 0.5 mm depth but smaller than the 1.5 mm pore diameter.

3.5 Comparison results and analysis

Through the comparative test, it was possible to derive the analysis above: the friction coefficient, wear quantity, and particle size of the abrasive particles all exhibit a declining tendency when the aperture diameter of the specimen filling pore increases. Along with a single adhesive wear mode, the wear form also offers a mixed wear mode that combines fatigue and adhesive wear. Therefore, 3 mm is chosen as the ideal filling pore diameter while taking into account the impact of the pore diameter factor on friction performance.

The friction coefficient swings steadily above and below a given value but tends to grow when the area distribution rate of the specimen filling pore increases. When the area distribution rate is 16%, the wear volume of the disk specimen is much higher than the earlier one. The degree of wear also increases along with the area distribution rate, and the particle size of the abrasive grains grows simultaneously. The particle size when the area distribution rate is 16% is much larger than the other two. Compared to the first two, the particle size is considerably greater, and the type of wear transitions from single adhesive wear to compound wear, which includes adhesive wear and fatigue wear. As a result, a 12% area distribution rate was chosen as the ideal area distribution rate for the filled pores while taking into account the impact of the area distribution rate on friction performance.

Both the quantity of wear and the coefficient of friction showed a trend of increasing and then decreasing as the depth of the filled pore rose. According to the amount of wear analysis of the specimens, the difference in friction performance between specimens with depths of 1 mm and 1.5 mm is insignificant, and the size of the mixed wear in the filled pore is the major reason for the difference. The particle size also increases and then decreases as the depth of the filled pore increases, and the form of wear changes from a single adhesive wear to a composite wear including adhesive wear and fatigue wear, and then from a composite wear to a single adhesive wear. As a result, when considering the effect of filling pore depth on friction performance, 0.5 mm is selected as the optimal filling pore depth.

4. CONCLUSION

In this paper, the effect of different filled pore structure sizes of tin bronze and 45 steel on tribological properties is investigated using graphite as a solid lubricant. The optimal filled pore structure parameters were determined by equivalence tests. The friction coefficients and the wear amounts under different structure parameters, were obtained in combination with orthogonal tests. The influence of the three parameters on the test results was obtained by orthogonal tests: the pore diameter of the filled pore > the area distribution rate > the depth of the filled pore. Finally, the optimal structure was determined as a 3 mm pore diameter, 12% area distribution rate, and 0.5 mm pore depth under the same conditions.

The effects of friction coefficient with time were studied for different pore diameters, different area distribution rates, and different pore depths within 1 hour. The average friction coefficients over 1 hour were: the largest for 2 mm pore diameter, the second largest for 2.5 mm, and the smallest for 3 mm pore diameter; the largest for 16% area distribution, the second largest for 14% area distribution, and the smallest for 12% area distribution; the largest for 1.5 mm pore depth, the second largest for 1 mm pore depth and the smallest for 0.5 mm pore depth.

When the effects of pore diameter on friction performance were investigated, it was discovered that the coefficient of friction, the amount of wear, and the particle size of the abrasive grains all showed a negative correlation with the pore diameter. All three decrease as the pore diameter increases, and the wear mode changes from mixed adhesive wear and fatigue wear to single adhesive wear. Through comparative analysis, the optimal filling pore size was determined to be 3 mm.

When all other conditions are held constant, the effect of the area distribution rate on friction performance is evaluated. The friction coefficient, wear amount, and particle size of the abrasive grains was positively correlated with the area distribution rate of the filled pores. All three showed an increasing trend as the specimen filling pore area distribution rate increased. The particle size of the abrasive particles is significantly larger than the first two when the area distribution rate is 16%. It also transitions

from single adhesive to composite wear, which includes adhesive and fatigue wear. Finally, an area distribution rate of 12% was chosen as the optimal area distribution rate of the filled pores.

As the depth of the specimen filling pores increases, the coefficient of friction and the amount of wear both tend to increase and then decrease with the rise in depth. The particle size of the abrasive particles shows a trend of increasing and falling. The wear form changes from single adhesive wear to compound wear, including adhesive wear and fatigue wear, with the increase of pore depth, and then changes from compound wear to single adhesive wear. After comparison and analysis, the filling pore depth of 0.5 mm was adopted as the optimal filling pore depth.

Acknowledgement

This research was carried out with the National Nature Science Foundation of China (No. 52175177) (Study on Solid Lubrication Wear Mechanism and Wear Characterization Method of Large Sliding Spherical Friction Pairs,2022.01-2025.12) and thanks for financial support of the National Nature Science Foundation of China(No. 52005292,2021.01-2023.12).

REFERENCES

[1] V.P. Sergeev, A.R. Sungatulin, M.P. Kalashnikov, O.V. Sergeev, M.T. Talgat, V.V. Neufeld, S. Yu. Zharkov, *Chevrel phase-based solid lubrication coating for wear resistant electrocontact friction pairs in vacuum*, Journal of Physics: Conference Series, vol. 154, 15th International Conference on Films and Coatings (ICFC 2021), 18-20 May, 2021, Saint Petersburg, Russia, doi: 10.1088/1742-6596/1954/1/012039

[2] P.N. Khopin, O.V. Kozlova, L.E. Gorbach, *Durability Evaluation for Friction Pairs with Solid Lubrication Coatings under Reverse Motion*, Journal of Friction and Wear, vol. 39, pp. 505-511, 2018 doi: 10.3103/s1068366618060053

[3] B. Chen, J. Zhang, J. Jia. W. Hu, C. Gong, *Tribological properties of solid lubricants (graphite, MoS_2) for Ni based materials*, IOP Conference Series: Earth and Environmental Science, vol. 186, 2018, doi: 10.1088/1755-1315/186/2/012030

[4] B.A. Eick, Z.R. Treece, B.F. Spencer Jr., M.D. Smith, S.C. Sweeney, Q.G. Alexander, S.D. Foltz, *Automated damage detection in miter gates of navigation locks*, Structural Control and Health Monitoring, vol. 25, iss. 1, 2018, doi: 10.1002/stc.2053

[5] Z. Xinze, W. Ruifeng, W. Jie, Z. Meiyun, *The Vibration Characteristics Analysis of Miter Gate Based on ANSYS Workbench and Vibration Test*, Applied Mechanics and Materials, vol. 380-384, pp. 64-68, 2013, doi: 10.4028/www.scientific.net/amm.380-384.64

[6] D.B. Hamilton, J.A. Walowit, C.M. Allen, *A theory of Lubrication by Microirregularities*, Journal of Basic Engineering, vol. 88, iss. 1, pp. 177-185, 1966, doi: 10.1115/1.3645799

[7] H. Yu, X. Wang, F. Zhou, *Geometric Shape Effects of Surface Texture on the Generation of Hydrodynamic Pressure Between Conformal Contacting Surfaces*, Tribology Letters, vol. 37, pp. 123-130, 2010, doi: 10.1007/s11249-009-9497-4

[8] X. Hua, J.C. Puoza, P. Zhang, J. Sun, *Friction properties and lubrication mechanism of self-lubricating composite solid lubricant on laser textured AISI 52100 surface in sliding contact*, International Journal of Surface Science and Engineering, vol. 12, no. 3, pp. 228-246, 2018, doi: 10.1504/ijsurfse.2018.094774

[9] S. Yang, J. Sun, Y. Gou, M. Zheng, S. Su, X. Wang, *Wear life prediction of cemented carbide microtextured surface*, Materials Science and Engineering, B, vol. 262, 2020, doi: 10.1016/j.mseb.2020.114685

[10] C.E. Morstein ,M. Dienwiebel, *Graphite lubrication mechanisms under high mechanical load*, Wear, vol. 477, 2021, doi: 10.1016/j.wear.2021.203794

[11] C. Qiujie, Y. Aibing, Z. Shuo, W. Maochao, Y. Jiandong, S. Lei, C. Jianying, *Effect of magnetic field on tribological performance of laser dimple textured surface*, Wear, vol. 468-469, 2021, doi: 10.1016/j.wear.2020.203584

[12] J. Suparno, D.A. Halim, J. Junadi, A. Setiawan, M. Effendy, J. Jamari, *Graphite as Dry Lubricant to Reduce Rail Wheels Wear Level*, Materials Science Forum, vol. 961, pp. 126-133, 2019 doi: 10.4028/www.scientific.net/msf.961.126

[13] G. Ryk, I. Etsion, *Testing piston rings with partial laser surface texturing for friction reduction*, Wear, vol. 261, iss. 7-8, pp. 792-796, 2006, doi: 10.1016/j.wear.2006.01.031

[14] X. Shi, T.W. Liskiewicz, B.D. Beake, J. Chen, C. Wang, *Tribological performance of graphite-like carbon films with varied thickness*, Tribology International, vol. 149, 2020, doi: 10.1016/j.triboint.2019.01.045

[15] A. Codrignani, B. Frohnapfel, F. Magagnato, P. Schreiber, J. Schneider, P. Gumbsch, *Numerical and experimental investigation of texture shape and position in the macroscopic contact*, Tribology International, vol. 122, pp. 46-57, 2018 doi: 10.1016/j.triboint.2018.02.001

[16] F. Guo, X. Jia, L. Wang, Y. Wang, *The effect of axial position of contact zone on the performance of radial lip seals with a texturing shaft surface*, Tribology International, vol. 97, 2016, doi: 10.1016/j.triboint.2016.01.031

[17] M. Leonardi, M. Alemani, G. Straffelini, S. Gialanella, *A pin-on-disc study on the dry sliding behavior of a Cu-free friction material containing different types of natural graphite*,Wear, vol. 442-443, 2020, doi: 10.1016/j.wear.2019.203157

[18] Z. Xinze, W. Xinghua, X. Xiang, Z. Zuyue, *Tribological properties of the bottom pivot friction pair of miter gate under graphite lubrication*, Lubrication Engineering, vol. 47, iss. 8, pp. 107-113, 2022, doi: 10.3969/j.issn.0254-0150.2022.08.015

[19] X. Zhao, D. Su, X. Xu, Y. Dong, Z. Gong, *Study on surface wear of gate bottom pivot based on multi-notch measurement*, Wear, vol. 462-463, 2020, doi: 10.1016/j.wear.2020.203519

[20] C. Calli, O. Tazegul, E.S. Kayali, *Wear and corrosion characteristics of copper-based composite coatings*, Industrial Lubrication and Tribology, vol. 69, iss. 2, pp. 300-305, 2017, doi: 10.1108/ILT-07-2016-0146

[21] L. Zhao, J. Li, Q. Yang, Y. Wang, X. Zhang, H. Li, Z. Yang, D. Xu, J. Liu, *Study on Friction and Wear Properties of New Self-Lubricating Bearing Materials*, Crystals, vol. 12, iss. 6, 2022, doi: 10.3390/cryst12060834

[22] H. Sarmadi, A.H. Kokabi, S.M. Seyed Reihani, *Friction and wear performance of Copper-Graphite surface composites fabricated by friction stir processing (FSP)*, Wear, vol. 304, iss. 1-2, 2013, doi: 10.1016/j.wear.2013.04.023

[23] K.-Y. Zhang, Y.-G. Yin, G.-T. Zhang, S.-G. Ding, Q. Chen, *Tribological Properties of FeS/Cu Copper-Based Self Lubricating Bearing Materials Prepared by Mechanical Alloying*, Tribology Transactions, vol. 63, iss. 2, pp. 197-204, 2019, doi: 10.1080/10402004.2019.1668515

[24] C. Chen, Q. Yang, Q. Chen, Y. Wang, D. Xu, H. Li, X. Zhang, C. M. Harvey, J. Liu, *Tribological properties of copper-embedded self-lubricating bearing materials*, Industrial Lubrication and Tribology, vol. 74, iss. 7, pp. 796-803, 2022, doi: 10.1108/ILT-03-2022-0067

[25] Y. Yanguo, L. Rongrong, Z. Guotao, Z. Kaiyuan, D. Shuguang, C. Qi, *Tribological properties of FeS/Cu-Bi copper-based bearing materials fabricated by mechanical alloying*, Industrial Lubrication and Tribology, vol. 71, iss. 10, pp. 1152–1157, 2019 doi: 10.1108/ilt-03-2019-0106

[26] P.S. Sarath, R. Reghunath, S. Thomas, J.T. Haponiuk, C.G. Soney, *An investigation on the tribological and mechanical properties of silicone rubber/graphite composites*, Journal of Composite Materials, vol. 55, iss. 26, 2021, doi: 10.1177/00219983211031634

[27] X. Xiang, Z. Zuyue, W. Xinghua, H. Baijun, Q. Hongling, Z. Xinze, *Experimental study on friction characteristics of miter gate bottom pivot with different solid lubrication*, Tribology, vol. 42, iss. 5, pp. 1044-1052, 2022, doi: 10.16078/j.tribology.2021202